Results in Engineering 29 (2026) 109035

Contents lists available at ScienceDirect

Results in Engineering

journal homepage: www.sciencedirect.com/journal/results-in-engineering

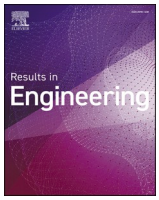

Effective thermal conductivity prediction model for vacuum insulation cores

Dron Kaushik [a], Anirudh Nunna [b], Harjit Singh [a,*]

[a] Department of Mechanical Engineering, College of Engineering, Design and Physical Sciences,Brunel University London, Uxbridge UB8 3PH, United Kingdom
[b] Department of Natural Sciences, University of Bath, Bath BA2 7AY, United Kingdom

ARTICLE INFO

Keywords:
Thermal conductivity
Vacuum insulation
Powder material
Finite element
MATLAB

ABSTRACT

Accurate prediction of thermal conductivity of porous granular materials enables the identification and rapid optimisation of new composite core materials for Vacuum Insulation Panels (VIPs). To date, no computer model has reported the use of multi-sized particles with a combined Finite Element Analysis (FEA) and Discrete Element Method (DEM) approach to predict thermal conductivity of VIP core. To fill this knowledge gap, we propose a FEA and DEM based thermal conductivity prediction model for powdery composites, particularly suited for VIPs. The geometry of the model was formed using random packing of multisized spherical particles using DEM and a MATLAB PDE-based thermal model solver was used to obtain a solution for the generated geometry. The model can predict effective thermal conductivity whilst accounting for the VIP-specific fundamental heat exchange phenomena. The results from the model are validated against those obtained from accompanying thermal conductivity measurements performed using the Transient Hot Wire method, with results falling within the error range for temperatures <491.15 K. Effective thermal conductivity of a perlite and Silicon Carbide (SiC) core at 0.1 mbar over a temperature range of 303 K to 803 K, with the proportion of perlite varying from 100 % to 50 % (by weight), as predicted by the model, is presented. The thermal conductivity of the 50 % perlite-50 % SiC composite had the lowest rate of increase of thermal conductivity of 46.3 %, with the value increasing from 12.1 mW m^{-1} K^{-1} at 303 K to 17.7 mW m^{-1} K^{-1} at 803 K.

1. Introduction

Powder based Vacuum Insulation Panels (VIPs) have been widely studied for their use in the built environment. For example, Alam et al. [1], Simmler et al. [2] and Brunner et al. [3] discussed the technological requirements and cost factors relevant for VIPs when used in buildings. Future scope has been described as well, especially by Alam et al. [1]. Verma et al. [4], Kaushik et al. [5] and Barton et al. [6] respectively investigated the use of VIPs in refrigerators, high temperature appliances (cooking ovens), and tokamak fusion reactors, specifically presenting the principles of core design. The properties of powdered materials are an important factor in deciding the thermal conductivity of the vacuum insulation panels. Experimental studies have used different materials available in the market to choose an optimally performing material composition to obtain a target thermal conductivity [7–13]. However, this approach was limited in its scope by the number of materials and their variants that could be tested due to time and cost factors.

A computer model would provide the flexibility to vary interfering factors such as particle size, pore size, density and extinction coefficient of materials to understand their effect on the thermal performance of VIPs in the most cost-effective manner. Rottmann et al. [14] used analytic equations to calculate the thermal conductivity of the perlite-based VIPs. Their model did not consider the variation in density, particle size, and packing of particles as the variables influencing solid and gaseous thermal conductivity. However, the experimental work in their study showed that density had a significant effect on the total thermal conductivity of the VIP. Verma and Singh [15] presented a thermal conductivity model with square and hexagonal close packing. However, the study assumed particles and pores to be mono-sized and did not consider radiative heat transfer. Jalali et al. [9] further developed the work done by Verma and Singh [15] and built a validated model for heat transfer processes in high temperature VIPs with radiative heat transfer considered. However, the particles and pores are still considered mono-sized, which is not the case in practical applications. Random Close Packing (RCP) can be used to overcome the limitations present in previously reported models like mono-sized particle and pore size and the effect of

* Corresponding author.
E-mail address: harjit.singh@brunel.ac.uk (H. Singh).

https://doi.org/10.1016/j.rineng.2026.109035
Received 12 October 2025; Received in revised form 4 January 2026; Accepted 6 January 2026
Available online 7 January 2026

Nomenclature

Symbol

A	Box height
H	Coupling factor
k	Thermal conductivity
K_g	Gaseous thermal conductivity of a pore
k_{gr}	Thermal conductivity of a porous perlite particle
k_p	Thermal conductivity of perlite solid matrix
L	Box length
λ_0	Thermal conductivity of free air
Q	Heat flux
r_{eq}	Equivalent pore radius
T	Temperature
θ	Perlite porosity
ν	k_p/K_g
Z	A constant
$\overline{x}$	Mean
σ	Standard deviation
ε_{ab}	Radiative power from a surface
σ	Stefan-Boltzmann's constant
λ_r	Radiative thermal conductivity
e_R^*	mass specific extinction coefficient
a	Area
n	Refractive index (real part)
C_1C_2	Constants
Λ	Wavelength
δ_i	Mass fraction of i^{th} element

Abbreviations

DEM	Discrete Element Method
FEA	Finite Element Analysis
FTIR	Fourier Transform Infrared
KBr	Potassium Bromide
PxSiCy	Target composition by weight, x % perlite and y % SiC
RCP	Random Close Packing
SiC	Silicon Carbide
THW	Transient Hot Wire
VIP(s)	Vacuum Insulation Panel(s)

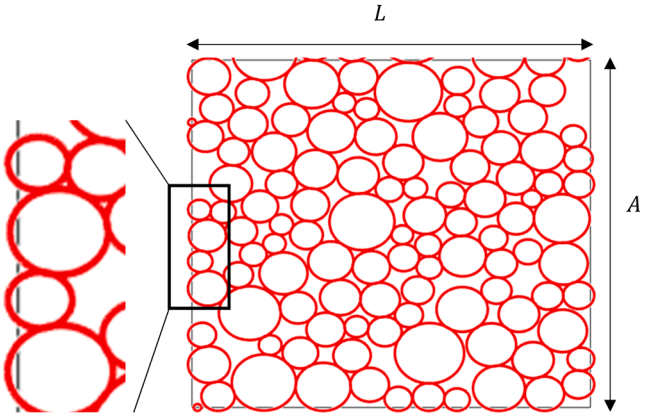

Fig. 1. Increase in model wall length due to the compressive (normal) forces caused by the packing particles on walls. A and L are horizontal and vertical dimensions of the packing box, respectively.

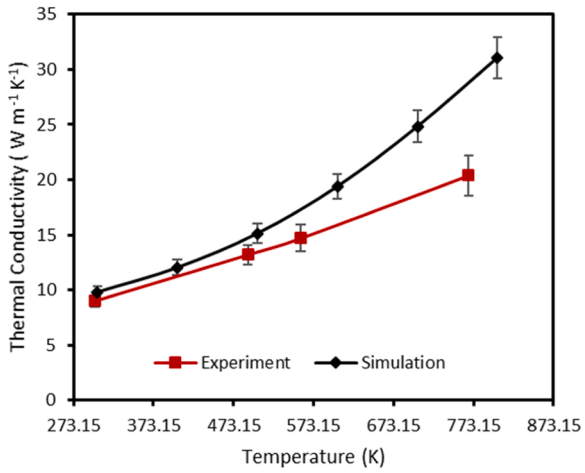

Fig. 2. Thermal conductivity of a perlite P100 sample at 0.1mbar determined from simulations and experimental measurements.

density. Numerous articles have been published in the literature on RCP algorithms to simulate the packing of spherical particles inside a bounded geometry [16–22]. Random packing algorithms can be categorised into two categories geometry-based and force/physics-based algorithms. Han et al. [17] used a geometric method to generate random packing of multisized particles. Fend et al. [23] used an advancing front method to generate discs in a box for discrete element method (DEM) based simulations. Many studies have reported the use of a random packing algorithm for thermal conductivity predictions for particle beds for various applications, like reactor beds [11]. Sahoo et al. [24] used FEA-DEM model to predict the thermal conductivity of pineapple wood based filled polymer composites. Thermal conductivity of the pineapple wood based composite dropped from 0.342 to 0.245 $Wm^{-1}K^{-1}$ with filler content increasing from 0 to ~18 %. Though his study used the FEA based model to predict the effective thermal conductivity, the role of vacuum (suppressed convective exchange and the play of gaseous conductivity) and the effect of radiation were not considered. Argento and Bouvard [25] showed that an increase in relative density leads to an increase in the effective thermal conductivity of the granular packings. Jayachandran and Reddy [26] have developed and validated an analytical model for packed particle beds in the temperature range of 373 K to 673 K. The effects of contact ratio, particle conductivity, porosity, and air pressure were studied, and an analytical model for predicting thermal conductivity in periodically packed beds was developed using the unit cell resistance method. The study conducted by Wang et al. [27] employed a coupled DEM-CFD-based model; however, it did not consider radiative exchange. Gan et al. [28] used the DEM approach to study conductive heat transfer in ellipsoidal particles and looked at the variation in thermal conductivity with aspect ratio and particle size. Their findings suggested an increase in thermal conductivity with an increase in temperature and a decrease in thermal conductivity with a decrease in particle size.

However, these studies were not directly focused on the VIP cores, which have significantly smaller pores and a thinner cross-section, causing the radiative mode to dominate other modes of heat transfer, especially at temperatures above 70 °C [5]. Previously published models for VIPs have not considered different compositions and particle size variation. These fail to predict and optimise the thermal conductivity of composite cores (cores with more than one material), which are used in every commercially available VIP globally.

In the current study, we use a DEM-based packing model developed by Rangel R [29] for 2-D circular particles. 2-D circular particles are

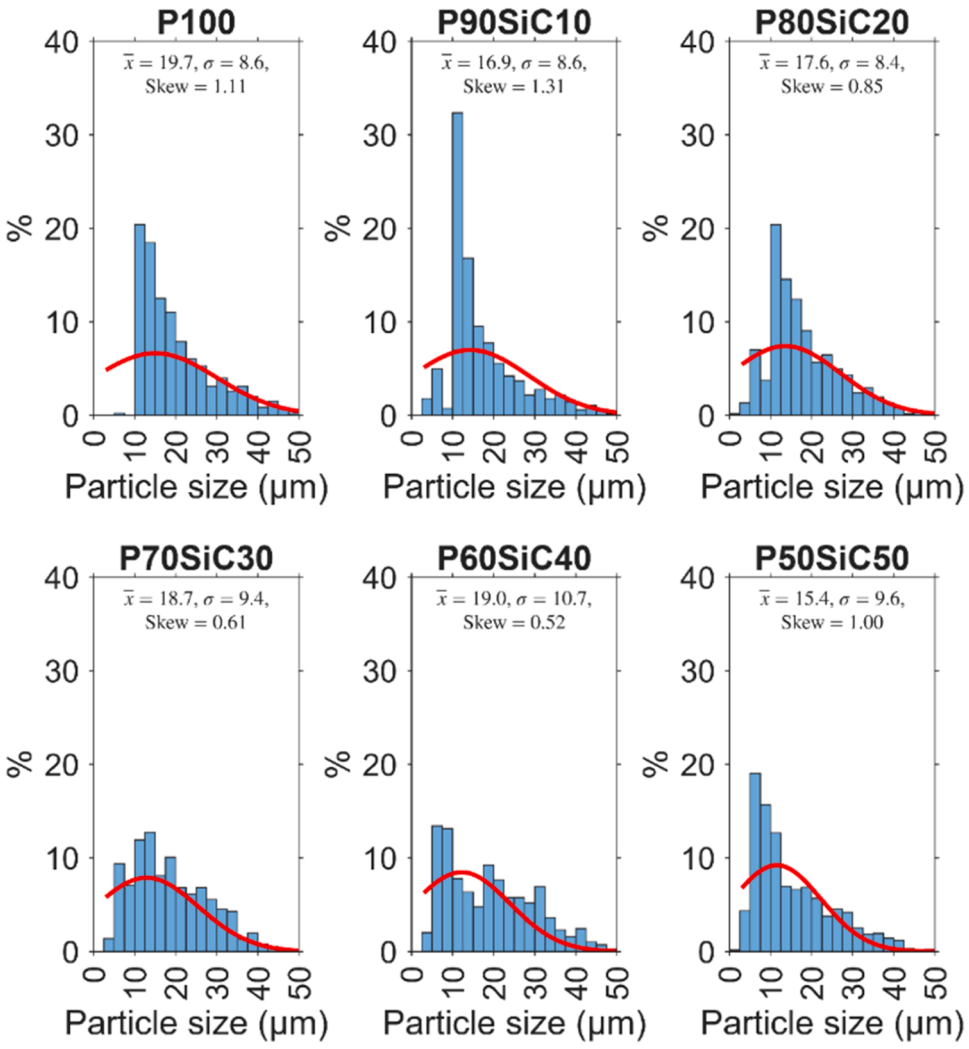

Fig. 3. Generated output particle size distribution (blue) and input particle size distribution (red) for different compositions of perlite and SiC composites. A bin size of 2.5 μm was used and the mean (x), standard deviation (σ) and skewness (skew) are shown for each output distribution in the subplot.

considered isotropic. Use of 2-D model is expected to lead to less computationally intensive simulations with minimal loss of accuracy, though there will be obvious differences in packing and pore networks in 2-D and 3-D cases. A nonlinear, viscoelastic model developed by Brilliantov et al. [30] and a nonlinear spring-dashpot with sliding friction model [31] are used to solve for the normal forces and tangential forces, respectively (See appendix equations A1-A4 for more). A square of 1500 μm was considered as a representative volume element, and the size of the box was decided for the particle size of <30 μm as described by Zeng et al. [32]. Where size of the box was decided to avoid the effect of walls on the filling geometry. From the generated packing, an FEA readable geometry was generated using MATLAB. An effective thermal conductivity of the packing was calculated based on the steady state Fourier's law for a mean temperature range of 303 K to 803 K at a pressure of 0.1 mbar. Radiative conductivity was added to the solution using the Mie model developed by Jalali et al. [9]. The model was employed to identify the effect of varying perlite-SiC compositions to find the properties for the lowest thermal conductivity. The model developed in this study is the first to employ DEM-FEA based random packing to predict thermal conductivities of VIP composite cores and optimise the core compositions for different operating/application temperatures.

2. General details of the model

The developed model used a DEM method to pack 2-D particles to create a packing with varying size distribution, following which FEA was employed to solve for the temperature field to predict effective thermal conductivity. Low pressure, small pore and particle sizes and specific material properties were used to make the model specifically suitable for use in the case of VIPs made with expanded perlite particles and SiC opacifier. The sections below describe the model construction and material properties in detail.

2.1. Packing and geometry creation strategy

The model creation consists of three main steps: particle generation, packing using the DEM based model and FEA based geometry creation. Once these steps are completed, boundary conditions are assigned for the solution.

The particle sizes and locations were generated using normal and uniform distributions, respectively. The radii were chosen randomly from a normal distribution with mean (x) and standard deviation (σ). Generated particle radii must lie within two standard deviations of the mean. Likewise, the locations were randomly chosen from a uniform distribution from zero to the maximum height or width of the box, depending on whether x or y coordinates were being chosen. The

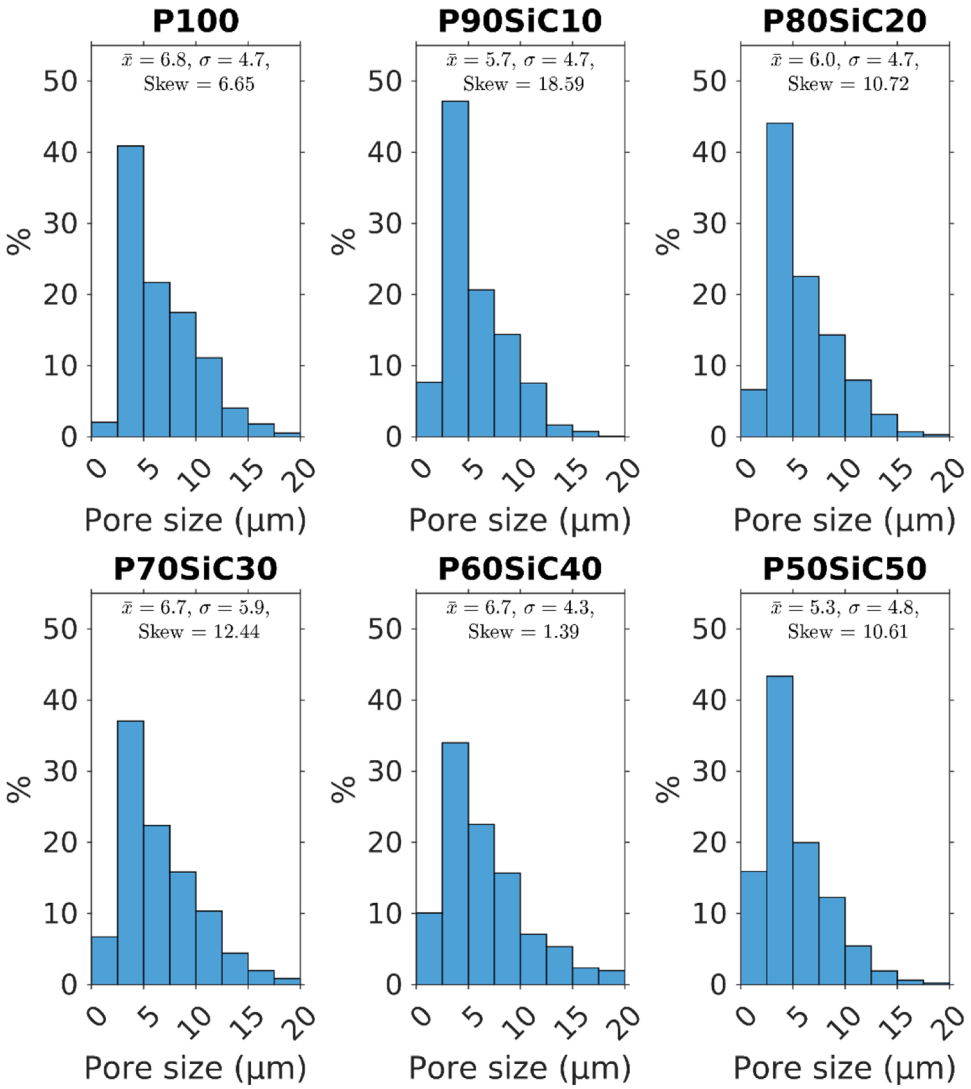

Fig. 4. Generated output interparticle pore size distribution for different compositions of perlite-SiC composites. A bin size of 2.5 μm was used and the mean ($\bar{x}$), standard deviation (σ) and skewness (skew) are shown for each subplot.

Table 1
Weight percentage of perlite in different compositions and the input and output packing compositions.

Compositions	Perlite weight input (%)	Perlite weight output (%)
P100	100	100
P90SiC10	90	93.12
P80SiC20	80	84.93
P70SiC30	70	76.55
P60SiC40	60	67.8
P50SiC50	50	51.77

initially generated particle distribution must have non-intersecting particles i.e., distance between two centres should be more than the sum of the radii of those two circles.

For bidisperse particles, the same process was used with a second normal distribution for the other phase. To control the relative weight proportion of both particles, the first phase was generated until a predetermined mass fraction was reached, and then the second. Then the particles were packed using the DEM method (script provided in the appendix) to obtain final position of particles.

This box full of particles must be converted into a FEA readable geometry before it can be used in thermal simulations, which was done using the inbuilt functions in MATLAB. Boundary conditions, such as temperature on either side of the box and material thermal conductivity were applied (Appendix Table A1), which were selected based on the application range of buildings and ovens/furnaces.

2.2. Material properties employed

Centre and radius data generated by the RCP algorithm of multisized spheres were used to create an analytical geometry for the MATLAB solver. Pristine perlite and a composite of perlite and SiC were studied. The area of the individual interparticle pore was calculated, and an equivalent radius was generated for the pore based on Eq. (1). Eq. (2) was used to calculate the gaseous thermal conductivity of a pore. The constants used in the equation shown in Eqs. (3)–6, derived from Rottmann et al. [33].

$$r_{eq} = \sqrt{\frac{Area}{\pi}} \tag{1}$$

$$K_g = H(T) * \left(\frac{\lambda_0(T)}{\left(1 + \left(\frac{Z(T)}{(2r_{eq} \times pressure)}\right)\right)} \right) \tag{2}$$

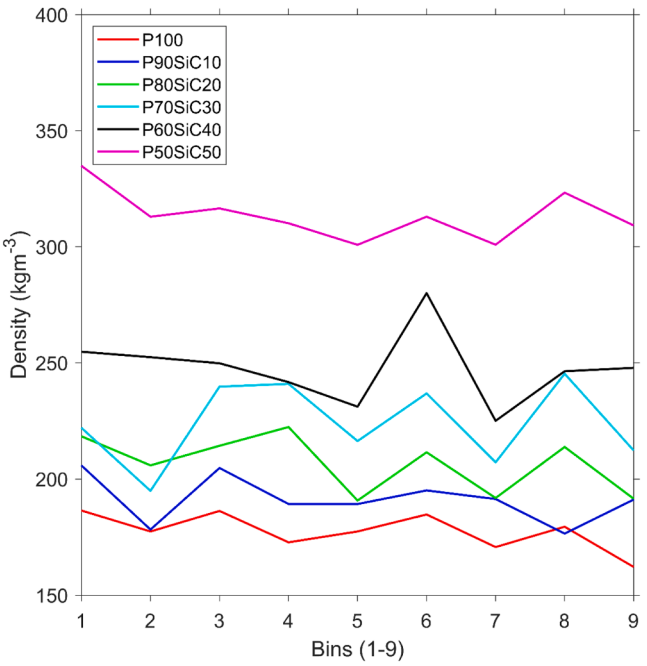

Fig. 5. Density variation with box height. The box has been divided in 9 equal bins with bin 1 at the bottom of the box and bin 9 at the top. A Bayesian correlation test has been conducted to test the correlation between height and density, where a strong correlation factor is defined as 0.7. All the compositions are well below the limit of 0.7, with 0.515 for P80SiC20 being the highest and 0.111 for P70SiC30 being the lowest. For more details, refer to Table A3 in the Appendix.

$$k_p = 0.75 \times \left(0.3049 + 0.006197 \times T - \left(1.153 \times 10^{-5}\right)T^2 + \left(1.034 \times 10^{-8}\right)T^3 - \left(3.352 \times 10^{-12}\right)T^4\right) \quad (3)$$

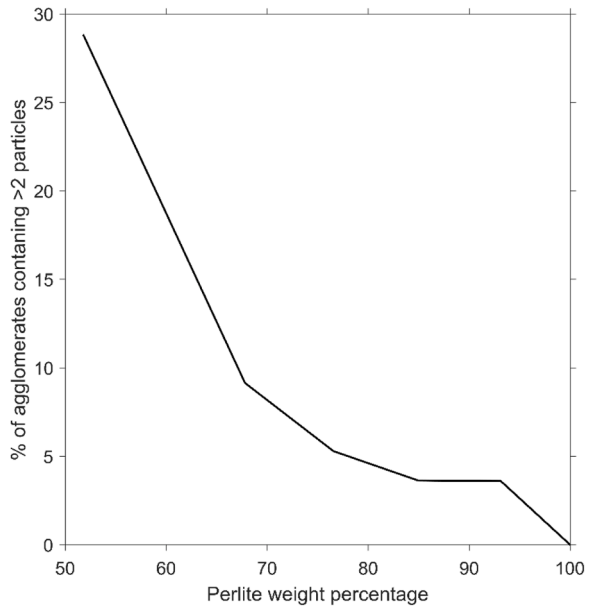

Fig. 7. Percentage of SiC agglomerates containing >2 particles at a cut-off distance of 5 μm.

$$Z(T) = \left(6.319 + 0.01526 \times T + 0.004045 \times T^2 - \left(2.468 \times 10^{-6}\right)T^3 + \left(6.326 \times 10^{-10}\right)T^3\right) \times 10^{-4} \quad (4)$$

$$\lambda_0(T) = \left(0.5180(T - 46.85)^{0.7104}\right) \times 10^{-3} \quad (5)$$

$$H(T) = 2.142 - 5.843 \times 10^{-4} \times T \quad (6)$$

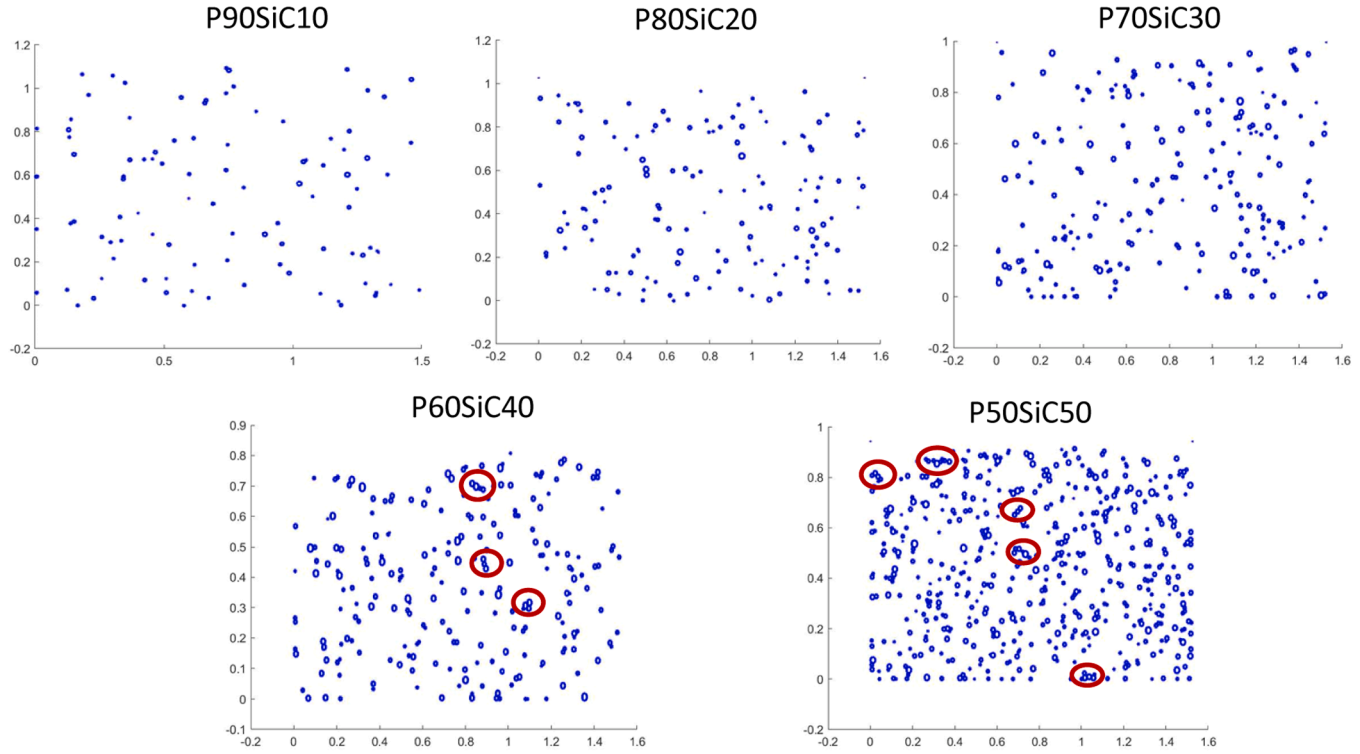

Fig. 6. Positions of SiC particles in the packing of various compositions as predicted by the model. As the weight percentage of SiC increases in the composition, the number and proximity of SiC particles increases forming linked agglomerates as highlighted by red circles.

Table 2
Post-packing density and packing efficiency of different compositions were modelled. Packing efficiency was calculated as the fraction of the total box area occupied by circles, providing a representation of interparticle porosity.

Composition	Density (kg/m^3)	Packing efficiency (%)
P100	165.2	83.8
P90SiC10	178.9	84.1
P80SiC20	195.4	84.1
P70SiC30	212.6	83.8
P60SiC40	231.6	85.7
P50SiC50	299.1	84.2

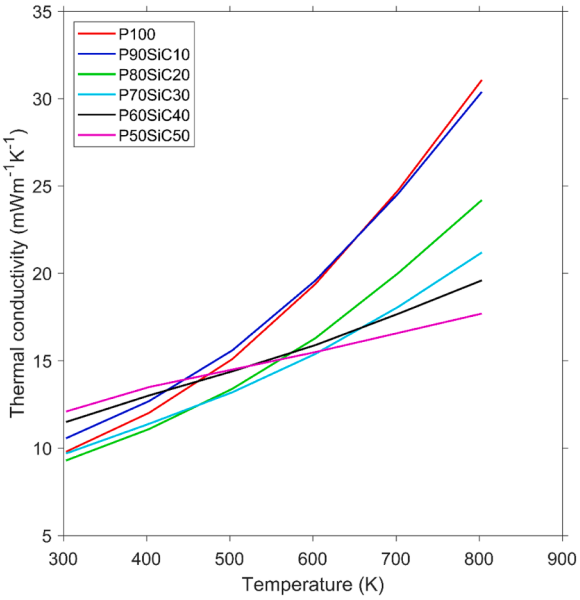

Fig. 8. Total thermal conductivity of core composites predicted by the model.

Thermal conductivity of Silicon carbide is calculated using Eq. (7).

$$k_{SiC} = 0.0004 \cdot T^2 - 0.8423 \cdot T + 529.3 \tag{7}$$

where r_{eq} is the equivalent radius of a pore and *Area* the cross-sectional area of a pore, T is the temperature, k_p the thermal conductivity of the perlite solid matrix, K_g the gaseous thermal conductivity of a pore, Z the combination of constants and parameters, λ_0 the thermal conductivity of free air and H is the coupling factor. The thermal conductivity of each particle was calculated using Eq. (8), known as Russel's equation. A porosity of 95 % was considered with an average pore size of 5 μm for a single particle of perlite.

$$K_{gr} = k_p \times \left(\frac{\theta^{2/3} + \nu\left(1 - \theta^{2/3}\right)}{\theta^{2/3} - \theta + \vartheta\left(1 - \theta^{2/3} + \theta\right)} \right) \tag{8}$$

where K_{gr} is the thermal conductivity of the porous perlite particle, θ the porosity of perlite and ν the ratio of k_p to K_g (k_p/K_g).

A pressure of 0.1 mbar was considered in all pores to calculate gaseous thermal conductivity using Eq. (2). The thermal conductivity of the pores and the solid matrix was considered to vary with the temperature as described in Eqs. (2)–8. The thermal conductivity values at the linear mean temperature were assigned to predict the effective thermal conductivity of the model, meaning the average of the temperature at the boundaries was used as an input in the equations above. The output for different boundary conditions was used as material properties. The effect of variation of the temperature inside the representative volume element was ignored to save computational cost, as it will have a minimal effect on the properties due small size and temperature difference.

The particles were compressed against the wall, and the length of the wall increases due to the forces exerted by the particles on the wall of the box, as seen in Fig. 1. This increases the length of the wall for boundary conditions. As each packing was different, the length of the wall for boundary conditions will be different for each packing. Hence, we cannot use the length (L) and height (A) of the wall as input box dimensions for determining thermal conductivity. To calculate the L/A ratio, we used a known thermal conductivity of 1 W m^{-1} K^{-1} for the materials in the geometry. The L/A ratio was independent of the thermal conductivity value used in the model, and it was calculated using Eq. (9). Further, Fourier's law was used for thermal conductivity calculations as shown in Eq. (10).

$$\left(\frac{L}{A}\right) = \frac{k \cdot \Delta T}{Q} \tag{9}$$

For thermal conductivity

$$k = \frac{Q \cdot L}{\mathrm{A} \cdot \Delta T} \tag{10}$$

where Q is the heat flux, ΔT the temperature difference between hot and cold surfaces and A and L the vertical and horizontal length of the geometry.

The mesh size was selected after a convergence study to be 69,303 elements with varying sizes as shown in the appendix (Figure A1). To check the effect of randomness in modelling results, a repeatability study was also conducted, shown in the appendix (Table A2).

2.3. Radiative conductivity

Rise in temperature leads to a rise in radiative heat transferred following Stefan-Boltzmann's law, Eq. (11).

$$\varepsilon_{ab} = \sigma a T^4 \tag{11}$$

where ε_{Ab} is the radiative power from a surface, σ the Stefan-Boltzmann's constant, a the area, T the temperature of the surface.

The radiative thermal conductivity of a diffusive material (optical thickness > 15) can be calculated using Eq. (12) [9,34].

$$\lambda_r = \frac{16\sigma n^2 T^3}{3\rho e_R^*(T_r)} \tag{12}$$

where λ_r is the radiative thermal conductivity, n the refractive index (real part), ρ the density of material, and e_R^* the mass specific extinction coefficient.

The mass specific extinction coefficient is the sum of absorption and scattering coefficients. In the current work, Mie scattering theory is used to obtain the spectral mass specific extinction coefficient [9] following which Eqs. (13) and 14 are used to calculate the mean mass specific extinction coefficient.

$$\frac{1}{e_R^*(T)} = \int_{\lambda_1}^{\lambda_2} \frac{1}{e_\Lambda^*(\Lambda)} \frac{\partial \varepsilon_{\Lambda b}}{\partial \varepsilon_b} \tag{13}$$

$$\frac{1}{e_R^*(T)} = \int_{\lambda_1}^{\lambda_2} \frac{1}{e_\Lambda^*(\Lambda)} \frac{\partial \varepsilon_{\Lambda b}}{\partial \varepsilon_b} \frac{\partial \varepsilon_{\Lambda b}}{\partial \varepsilon_b} = \frac{\pi C_1 C_2}{2\Lambda^6 \varepsilon_b^{5/4}} \frac{\exp\left[(C_2/\Lambda)(\sigma/\varepsilon_b)^{1/4}\right]}{\left\{\exp\left[(C_2/\Lambda)(\sigma/\varepsilon_b)^{1/4} - 1\right]\right\}^2} \tag{14}$$

where $\varepsilon_b = \varepsilon_{Ab}/A$, C_1 and C_2 are constants and e_Λ^* is the spectral mass specific extinction coefficient. To obtain the effective spectral mass specific extinction coefficient for composite cores we used Eq. (15).

$$e_{\Lambda,eff}^* = \sum_1^n \delta_i e_{\Lambda,i}^* \tag{15}$$

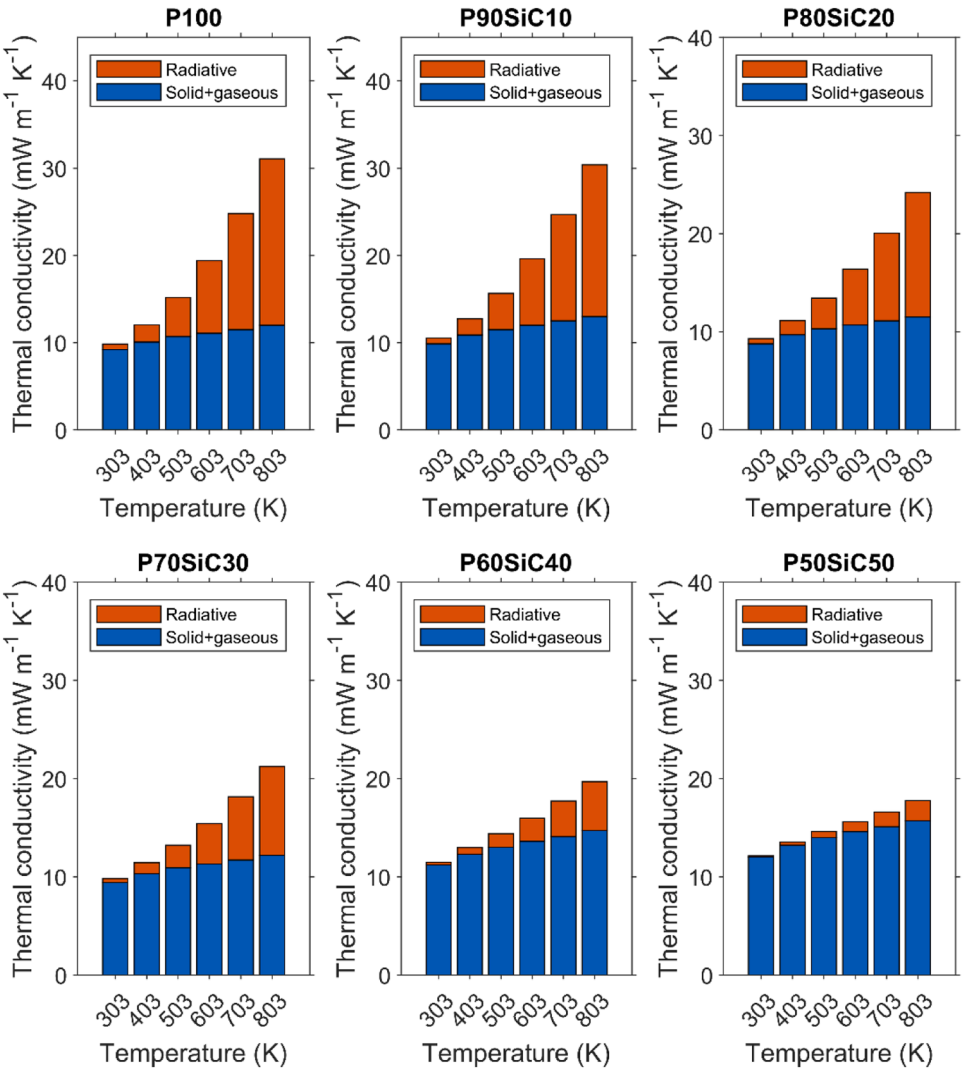

Fig. 9. Radiative (orange) and solid+gaseous (blue) thermal conductivities predicted by the model.

where $e^*_{\Lambda,eff}$ is the effective spectral mass specific extinction coefficient of the composite material, n the number of components in the powder composite, δ_i mass fraction of the i^{th} material and $e^*_{\Lambda,i}$ the spectral extinction coefficient of the i^{th} material.

A wavelength range of 2 μm to 20 μm is considered for the calculations. Accordingly, IR transmission spectra of perlite and SiC particles are also measured in that wavelength range using KBr pellet method.

Radiative heat exchange is considered parallel to the solid and gaseous conduction. The density and composition, as input parameters, are taken from the generated FEA-DEM geometry. Hence, the solid and gaseous thermal conductivity obtained from the FEA solution of the generated geometry is added to the radiative thermal conductivity calculated using Eq. (12). This provides the total thermal conductivity of the composite core.

3. Validation

The Transient Hot Wire (THW) method was used to experimentally measure the thermal conductivity of perlite samples and validate the results from the model. THW method has been used to measure the thermal conductivity of solids and liquids under varying pressures and temperatures [35–41]. The thermal conductivity of P100 sample (density 150 ± 5 kg/m^3) was measured at 0.1 mbar and four temperatures (299.9 K, 491.15 K, 557.15 K, 767.15 K) and compared against those predicted by the model, see Fig. 2. Results were found to be within the error range up to 491.15 K. The rate of increase of thermal conductivity was different for the experimental and predicted thermal conductivity, with the predicted being higher. This could be attributed to the under-measurement of radiative thermal conductivity by THW method as shown by Rottmann et al. [41]. The error in thermal conductivity measurement in THW method was calculated using the extinction coefficient of the sample. For this study, we used KBr pellet and transmission FTIR to collect quantitative spectral data. As the KBr method does not consider back scattering by particles, this will underpredict the extinction coefficient in the spectral range where particle size and the wavelength are of the same order and will not consider the effect of change in particle density [42]. This underprediction causes the rate of increase in the predicted thermal conductivity to rise, while THW is not able to account for the underprediction of thermal conductivity. This double effect causes the measured and predicted thermal conductivity values to deviate at elevated temperatures, above 491.15 K in this study, as shown in Fig. 2. Future modellers can use infrared spectral data collected using the integrated sphere technique as described by Kuhn et al. [42]. A minimum deviation of 7.4 % was observed between experimental and simulation data for 303.15 K mean temperature and a maximum deviation of 30.7 % was observed for mean temperature of 803.15 K.

The proposed model can minimise the number of experiments

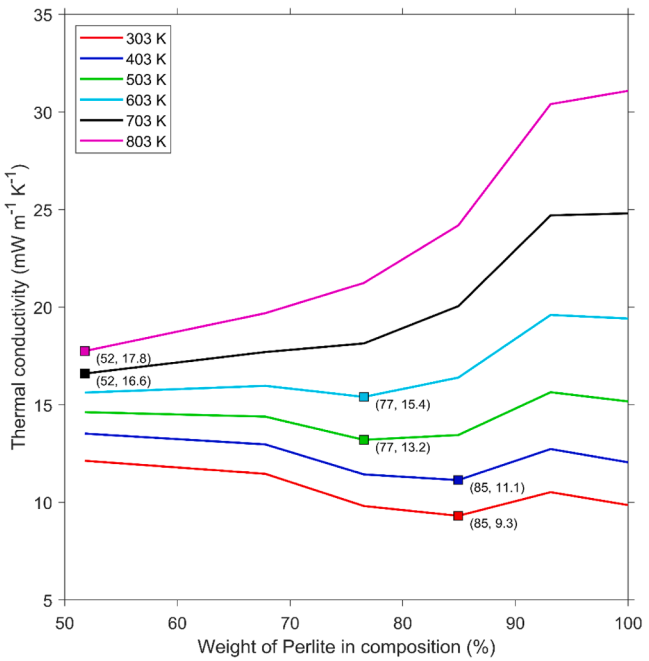

Fig. 10. Overall thermal conductivity of the core composites with varying amounts of perlite; the optimum compositions move to a lower SiC percentage with decreasing temperature. The optimal composition for each temperature is marked and listed as (Weight proportion of perlite in composition, Thermal conductivity).

required to determine an optimal composition for a given particle size of the spherical perlites and SiC. Readers should keep in mind the limitations of using 2-D circular particles and FTIR data measured using the KBr pellet method. The model was validated for one composition due to the expensive experimental measurements at high temperatures. Guarded Hot Plate (GHP) method can also be used to validate thermal conductivity measurements presented here. Commercially available GHPs can offer an accuracy of ~2 % irrespective of the extinction coefficients of the materials being tested. But the cost of testing using a GHP is much higher than that incurred when using THW equipment. Thermal conductivity measurements reported by Rottmann et al. [14] were performed using GHP equipment, which were of the same order as those provided in Fig. 2. The variation between the results is attributed to the different grades of perlites used in both studies. Further validation of the model with more compositions can be prioritised for future work.

4. Model results and discussion

The effect of particle size distribution and the composition of the core material was investigated, and temperature-dependent thermal conductivity was predicted to identify temperature specific optimal compositions. Particles were considered to have a spherical shape (circular for 2-D). It is understood that SiC and perlite may have a more angular/irregular shape in practical applications, which may affect the conductive heat transfer phenomenon as the contact between two particles changes.

4.1. Pore and particle size distribution

The compositions with 100 % perlite (pristine perlite) to 50 % perlite-50 % SiC were generated with a 10 % step change. Since the model follows a random approach to generate the packing the exact weight ratios of the materials cannot be achieved as input. Hence, an understanding must be developed of the finally achieved weight ratio of perlite and SiC. The output particle and pore size distribution were also studied to ensure the desired material properties in the packing were achieved. Fig. 3 and Fig. 4 show the particle size and pore size distribution for various packings. The input distribution of the P100 (see Table 1) was a normal distribution with a mean value of 30 μm and a standard deviation of 15 μm. The output particle size was not a normal distribution, as the initial packing scheme with no overlapping would favour smaller particle sizes as the box filled up. This skew towards smaller particle sizes is shown in Fig. 3. This skew towards smaller particles of perlite occurred less when the proportion (by weight) of the perlite was lower. Hence, in the case of P80SiC20, P70SiC30 and P60SiC40 we observed an increase in mean particle size and a decrease in the measure of skewness, as shown in Fig. 3, as more perlite particles were generated according to normal distribution. This particle generation and packing algorithm introduced a deviation between input and output proportions of perlite and SiC as seen in Table 1.

As the proportion of SiC in the composition increased, the number of smaller particles in the packing proportionately increased as the mean particle size of SiC used was 8 μm with a standard deviation of 3 μm. Interparticle pore sizes in the packing reduced with increasing SiC proportion, reducing the gaseous conduction. Reduction in average pore size can be attributed to the migration of smaller SiC particles into larger interparticle pores.

The SiC particles were denser, which means if the model was not able to control packing parameters, they could settle at the bottom of the packing. The settlement of heavier particles was avoided using random initial placement of particles and using high friction and damping factors in the DEM simulation. To confirm this quantitatively, we divided the box into 9 bins in the vertical direction. The density variation with bins for each packing is shown in Fig. 5. Density showed minimal to no specific trend and variation with height, showing that there was no settlement of particles.

The distribution of SiC particles within the packing was visualised, to ensure uniformity, after the packing was finished for all compositions, as shown in Fig. 6. It shows that as the weight ratio of SiC increases in the composition, they form "linked agglomerates" (circled in Fig. 6) after their concentration exceeds a certain threshold. This leads to an increase in the overall solid conductivity, due to a larger area of the packing being high conductivity. For perlite and SiC with mean particle size of 30 μm and 8 μm respectively the threshold comes between a perlite weight ratio of 76.55 % and 67.8 % as the solid thermal conductivity increases, as shown in Fig. 9.

To quantitatively measure the "linked agglomeration" of particles, we used a clustering algorithm to identify different clusters of SiC particles. Fig. 7 shows the proportion of agglomerates with a size of >2 particles at a cut-off distance of 5 μm. Linked agglomeration increased sharply for composites containing <70 % perlite, such as P60SiC40 and P50SiC50, which explains the increase in the solid+gaseous thermal conductivity for these compositions. Furthermore, this also explains the low thermal conductivity of composites containing ≥70 % perlite, such as P70SiC30, as predicted by the model.

4.2. Effect of composition and temperature

A range of pre-determined weight proportions of the perlite and SiC were used to obtain different target compositions of the VIP cores and the post packing parameters were calculated as shown in Table 2. The density of Perlite particles is considered as 200 kg/m^3 and the density of the SiC particle is considered as 2000 kg/m^3.

The rate of increase of the total thermal conductivity of the core decreased as the proportion of SiC increased, because SiC has a higher density and extinction coefficient than perlite (Fig. 8). Whereas radiative conductivity simply decreases with rising core density and extinction coefficient, Fig. 9, the variation of solid+gaseous conductivity with changing SiC weight proportion is a complex phenomenon; SiC particles have a higher solid thermal conductivity than perlite particles (Eq. (7)) [41]. Similar results have been reported by Verma et al. [7], who studied

the effect of adding different opacifiers to perlites up to 70 °C. This highlights the need for identifying the optimal proportions of SiC and perlite for the core to have a minimum overall thermal conductivity. According to Jalali et al. [9] as the density of the core increased, the solid+gaseous conductivity increased as well due to denser and less porous perlite particles, which have a higher solid conductivity based on Eq. (8). However, in the current study, the core density did not increase due to denser perlite particles, but rather due to the presence of SiC particles in the packing. These SiC particles were smaller in size (mean diameter 8 μm), and consequently, a greater number of them were able to be filled in the core composite. Such a packing is expected to offer a more tortuous path for heat flow when there are fewer SiC particles or none. SiC particles partake a smaller volume in the packing and are scattered in the whole packing space, leading to a lower rise in the solid+gaseous conductivity (Fig. 6). We observe a sudden increase in solid+gaseous conductivity when SiC proportion increases from 30 % (sample P70SiC30) to 40 % (sample P60SiC40). This is attributed to "agglomeration/clustering" of SiC particles as shown in Fig. 7, with P70SiC30 showing 5.2 % and P60SiC40 showing 9.2 % agglomeration. The optimal proportion of perlite and SiC particles by weight for a minimum core thermal conductivity was predicted to be 3.26:1 for the temperatures of 503 K and 603 K in the output geometry, as shown in Fig. 10. For temperatures above 603 K, P50SiC50 shows the lowest thermal conductivity. For temperatures lower than 503 K, P80SiC20 was found to be the optimum composition. This phenomenon of a decrease in solid+gaseous thermal conductivity with the addition of SiC in perlite-based VIPs was also observed in [7].

The solid thermal conductivity of the SiC particles decreases as temperature rises, and the rate of increase of solid+gaseous thermal conductivity of perlite also decreases with the increase in temperature, leading to perlite-SiC composites achieving a lower rate of increase in solid+gaseous conductivity at higher temperatures. The model was able to predict this behaviour, as shown in Fig. 9. The highest increase in solid+gaseous thermal conductivity with temperature was predicted for P100 composition (pristine perlite), with thermal conductivity increasing from 9.8 mW m^{-1} K^{-1} at 303 K to 31.08 mW m^{-1} K^{-1} at 803 K, a rise of 217.1 %. The lowest increase in the thermal conductivity was observed for P50SiC50, from 12.1 mW m^{-1} K^{-1} at 303 K to 17.7 mW m^{-1} K^{-1} at 803 K, a rise of 46.3 %. The increase in thermal conductivity for the intermediate composition P70SiC30 was 118 %, from 9.7 mW m^{-1} K^{-1} at 303 K to 21.2 mW m^{-1} K^{-1} at 803 K. There was a slight increase in the thermal conductivity of P90SiC10 compared to P100 at lower temperatures, but it lies within the repeatability error range of the simulation (±5.6 %) as shown in appendix (Table A2). The deviation in results occurred due to the random generation of packing.

For compositions with higher perlite and lower SiC weight proportions, the increase in the overall thermal conductivity with rising temperature was due to the increase in the radiative component. Caps et al. [43] found a similar trend. On the other hand, for composites with lower perlite and higher SiC proportions, the overall thermal conductivity increase was largely contributed by increased solid+gaseous conductivity. For example, 65.8 % of the increase in the overall thermal conductivity from 303 K to 803 K was contributed by solid conductivity for P50SiC50 composite as opposed to 13.2 % for P100 material, as shown in Fig. 9.

5. Conclusions

A random packing-based effective thermal conductivity prediction model to predict the optimum composite mix for vacuum insulation panels is presented. The model is unique on account of its capabilities to predict effective thermal conductivity of powder based vacuum insulation cores using a combination of DEM and FEA methods. It enables the understanding and evaluation of the effect of properties like particle size, density, temperature and material compositions on the increase of thermal conductivity components. As an example, perlite-SiC composite VIP cores were simulated to identify an optimum core composition for a given operation temperature, with the modelled results validated against experimental results obtained using the THW method. The P70SiC30 sample with SiC weight percentage of 23.45 % was predicted to have the lowest solid+gaseous and overall thermal conductivity over the range of 300 K to 603 K, and the P50SiC50 sample over 703 K to 803 K. This is attributed to the lower radiative conductivity for the compositions with higher proportions of opacifier. This effect of the opacifier is likely to be predominant at higher temperatures, where radiative conductivity is significantly higher. The developed model could help reduce the number of expensive experiments that are otherwise needed to develop new VIP core compositions. The model is capable of designing VIP core compositions suitable for applications across different temperature ranges, such as cooking ovens (50 – 500 °C), furnaces (>100 °C), refrigeration (−25 to 80 °C) and buildings (< 50 °C). Further work is proposed to extend the model's capabilities to include different 3-D particle shapes (e.g. ellipsoids), which are closer to real particles.

CRediT authorship contribution statement

Dron Kaushik: Writing – review & editing, Writing – original draft, Visualization, Validation, Software, Methodology, Investigation, Formal analysis, Conceptualization. **Anirudh Nunna:** Writing – review & editing, Software, Methodology, Investigation. **Harjit Singh:** Writing – review & editing, Supervision, Resources, Project administration, Funding acquisition.

Declaration of competing interest

The authors declare the following financial interests/personal relationships which may be considered as potential competing interests:

Corresponding author reports financial support was provided by British Council. Corresponding author reports financial support was provided by India's SPARC Programme. If there are other authors, they declare that they have no known competing financial interests or personal relationships that could have appeared to influence the work reported in this paper.

Acknowledgements

The authors would like to acknowledge the funding received from India's SPARC project (ID 2066) and British Council's ISPF research collaboration programme for PhotoHy. We would also like to acknowledge the Experimental Techniques Centre (ETC) at Brunel University for their support in providing FTIR equipment.

Supplementary materials

Supplementary material associated with this article can be found, in the online version, at doi:10.1016/j.rineng.2026.109035.

Data availability

Data will be made available on request.

References

[1] M. Alam, H. Singh, M.C. Limbachiya, Vacuum insulation panels (VIPs) for building construction industry - a review of the contemporary developments and future directions, Appl. Energy 88 (2011) 3592–3602, https://doi.org/10.1016/J.APENERGY.2011.04.040.

[2] H. Simmler, S. Brunner, Vacuum insulation panels for building application, Energy Build 37 (2005) 1122–1131, https://doi.org/10.1016/j.enbuild.2005.06.015.

[3] S. Brunner, K. Ghazi Wakili, T. Stahl, B. Binder, Vacuum insulation panels for building applications—continuous challenges and developments, Energy Build. 85 (2014) 592–596, https://doi.org/10.1016/j.enbuild.2014.09.016.

[4] S. Verma, H. Singh, Vacuum insulation panels for refrigerators, Int. J. Refrig. 112 (2020) 215–228, https://doi.org/10.1016/j.ijrefrig.2019.12.007.

[5] D. Kaushik, H. Singh, S.A. Tassou, Vacuum insulation panels for high-temperature applications – design principles, challenges and pathways, Therm. Sci. Eng. Prog. 48 (2024) 102415, https://doi.org/10.1016/j.tsep.2024.102415.
[6] P. Bartoň, P. Holejšovská, M. Šebík, Varju J. Fuková, Thermal testing of high-temperature vacuum insulations for tokamak COMPASS-U, Fusion Eng. Des. 219 (2025) 115259, https://doi.org/10.1016/J.FUSENGDES.2025.115259.
[7] S. Verma, A. Sara, H. Singh, Why and which opacifier for perlite based vacuum insulation panels (VIPs) in the average temperature range of 10–70 °C, Int. J. Therm. Sci. 186 (2023) 108136, https://doi.org/10.1016/j.ijthermalsci.2022.108136.
[8] T. Raad, S. Verma, H. Singh, Tree waste based advanced thermal insulation – vacuum insulation panels – for application at up to 70 °C, Int. J. Therm. Sci. 200 (2024) 108971, https://doi.org/10.1016/J.IJTHERMALSCI.2024.108971.
[9] Jalali MR, D. Kaushik, S. Verma, H. Singh, A coupled model of finite element method and Mie theory for heat transfer inside expanded perlite vacuum insulation panels (VIPs) at high temperatures, Int. J. Heat Mass Transf. 219 (2024) 124885, https://doi.org/10.1016/j.ijheatmasstransfer.2023.124885.
[10] Li CD, M.U. Saeed, N. Pan, Z.F. Chen, T.Z. Xu, Fabrication and characterization of low-cost and green vacuum insulation panels with fumed silica/rice husk ash hybrid core material, Mater Des. 107 (2016) 440–449, https://doi.org/10.1016/J.MATDES.2016.06.071.
[11] X.D. Wang, .D Sun, Y.Y. Duan, Z.J. Hu, Radiative characteristics of opacifier-loaded silica aerogel composites, J. Non Cryst. Solids 375 (2013) 31–39, https://doi.org/10.1016/J.JNONCRYSOL.2013.04.058.
[12] G. Wei, Y. Liu, X. Zhang, F. Yu, X. Du, Thermal conductivities study on silica aerogel and its composite insulation materials, Int. J. Heat Mass Transf. 54 (2011) 2355–2366, https://doi.org/10.1016/j.ijheatmasstransfer.2011.02.026.
[13] F. Wang, X. Xia, C. Sun, Experimental investigation of high-temperature insulation performance of vacuum encapsulated ceramic fiber-board, Therm. Sci. Eng. Prog. 47 (2024) 102369, https://doi.org/10.1016/J.TSEP.2023.102369.
[14] M. Rottmann, T. Beikircher, H.-P. Ebert, F. Hemberger, J. Manara, Thermal conductivity and extinction coefficient of opacified expanded perlite for vacuum super insulation up to 1073 K, Int. J. Therm. Sci. 163 (2021) 106813, https://doi.org/10.1016/j.ijthermalsci.2020.106813.
[15] S. Verma, H. Singh, Predicting the conductive heat transfer through evacuated perlite based vacuum insulation panels, Int. J. Therm. Sci. 171 (2022) 107245, https://doi.org/10.1016/J.IJTHERMALSCI.2021.107245.
[16] To HD, S.A. Galindo-Torres, A. Scheuermann, Sequential sphere packing by trilateration equations, Granul Matter 18 (2016) 70, https://doi.org/10.1007/s10035-016-0666-5.
[17] K. Han, Y.T. Feng, D.R.J Owen, Sphere packing with a geometric based compression algorithm, Powder Technol. 155 (2005) 33–41, https://doi.org/10.1016/j.powtec.2005.04.055.
[18] R.Y. Yang, R.P. Zou, A.B. Yu, S.K. Choi, Pore structure of the packing of fine particles, J. Colloid Interface Sci. 299 (2006) 719–725, https://doi.org/10.1016/J.JCIS.2006.02.041.
[19] Hall JR, S.K. Kauwe, T.D. Sparks, Sequential machine learning applications of particle packing with large size variations, Integr. Mater. Manuf. Innov. 10 (2021) 559–567, https://doi.org/10.1007/S40192-021-00230-7/FIGURES/8.
[20] Z. Chen, Y. Zhao, A quasi-physical method for random packing of spherical particles, Powder Technol. 412 (2022) 118002, https://doi.org/10.1016/J.POWTEC.2022.118002.
[21] H.S. Elmsahli, I.C Sinka, A discrete element study of the effect of particle shape on packing density of fine and cohesive powders, Comput. Part Mech. 8 (2020), https://doi.org/10.1007/s40571-020-00322-9.
[22] X. Wang, Z.Y. Yin, D. Su, X. Wu, J. Zhao, A novel approach of random packing generation of complex-shaped 3D particles with controllable sizes and shapes, Acta Geotech 17 (2022) 355–376, https://doi.org/10.1007/S11440-021-01155-3/FIGURES/24.
[23] Y.T. Feng, K. Han, D.R.J. Owen, Filling domains with disks: an advancing front approach, Int. J. Numer Methods Eng. 56 (2003) 699–713, https://doi.org/10.1002/nme.583.
[24] B. Sahoo, P. Pradhan, A. Purohit, H. Jena, B.B. Sahoo, Dielectric and thermal behavior analysis of polyester composites filled with pineapple wood dust using finite element method, Int. J. Polym. Anal. Charact. 30 (2025) 666–674, https://doi.org/10.1080/1023666X.2025.2496319.
[25] C. Argento, D. Bouvard, Modeling the effective thermal conductivity of random packing of spheres through densification, Int. J. Heat Mass Transf. 39 (1996) 1343–1350, https://doi.org/10.1016/0017-9310(95)00257-X.
[26] S. Jayachandran, K.S Reddy, Estimation of effective thermal conductivity of packed beds incorporating effects of primary and secondary parameters, Therm. Sci. Eng. Prog. 11 (2019) 392–408, https://doi.org/10.1016/j.tsep.2018.12.011.
[27] C. Wang, L. Chen, S. Liu, A DEM-CFD numerical model for the prediction of the effective thermal conductivity of pebble beds with contact conduction, Fusion Eng. Des. 147 (2019) 111257, https://doi.org/10.1016/j.fusengdes.2019.111257.
[28] J. Gan, Z. Zhou, A. Yu, Effect of particle shape and size on effective thermal conductivity of packed beds, Powder Technol. 311 (2017) 157–166, https://doi.org/10.1016/j.powtec.2017.01.024.
[29] R.L. Rangel, DEMLab: a Discrete Element method development environment, Softw. Impacts 21 (2024) 100670, https://doi.org/10.1016/j.simpa.2024.100670.
[30] N.V Brilliantov, F. Spahn, J.-M. Hertzsch, T. Pöschel, The collision of particles in granular systems, Phys. A: Stat. Mech. Appl. 231 (1996) 417–424, https://doi.org/10.1016/0378-4371(96)00099-4.
[31] F. DIMAIO, A. DIRENZO, Modelling particle contacts in distinct element SimulationsLinear and non-linear approach, Chem. Eng. Res. Des. (83) (2005) 1287–1297, https://doi.org/10.1205/cherd.05089.
[32] J. Zeng, K.M. Chung, X. Zhang, S. Adapa, T. Feng, Y. Pei, et al., Thermal conductivity modeling of monodispersed microspheres using discrete element method, J. Appl. Phys. 130 (2021) 165104, https://doi.org/10.1063/5.0056786.
[33] M. Rottmann, T. Beikircher, Pressure dependent effective thermal conductivity of pure and SiC-opacified expanded perlite between 293 K and 1073 K, Int. J. Therm. Sci. 179 (2022) 107652, https://doi.org/10.1016/J.IJTHERMALSCI.2022.107652.
[34] J. Kim, K. Kim, K. Bae, K.J. Juhn, J.S Kang, Exploring the ultralow effective thermal conductivity of hollow glass microsphere at various pressures and temperatures, Int. J. Heat Mass Transf. 230 (2024) 125784, https://doi.org/10.1016/J.IJHEATMASSTRANSFER.2024.125784.
[35] X. Zheng, Y. Bao, D. Qu, J. Wu, G. Qin, Y. Liu, Thermal conductivity measurements for long-chain n-alkanes at evaluated temperature and pressure: n-dodecane and n-tetradecane, J. Chem. Thermodyn. 162 (2021) 106566, https://doi.org/10.1016/j.jct.2021.106566.
[36] A. Huang, Y. Bao, H. Li, Y. Liu, X. Zheng, G. Qin, Thermal conductivity of ethylene glycol and water binary mixtures at evaluated temperature and pressure, J. Chem. Thermodyn. 175 (2022) 106900, https://doi.org/10.1016/j.jct.2022.106900.
[37] X. Zheng, Y. Bao, D. Qu, Y. Liu, G. Qin, Measurement and modeling of thermal conductivity for short chain methyl esters: methyl butyrate and methyl caproate, J. Chem. Thermodyn. 159 (2021) 106486, https://doi.org/10.1016/j.jct.2021.106486.
[38] Wei LC, L.E. Ehrlich, Powell-Palm MJ, C. Montgomery, J. Beuth, J.A. Malen, Thermal conductivity of metal powders for powder bed additive manufacturing, Addit. Manuf. 21 (2018) 201–208, https://doi.org/10.1016/j.addma.2018.02.002.
[39] H. Ebert, V. Bock, O. Nilsson, J. Fricke, The hot-wire method applied to porous materials of low thermal conductivity, High Temp.-High Press. 25 (1993) 391–402.
[40] R. Coquard, D. Baillis, D. Quenard, Experimental and theoretical study of the hot-wire method applied to low-density thermal insulators, Int. J. Heat Mass Transf. 49 (2006) 4511–4524, https://doi.org/10.1016/J.IJHEATMASSTRANSFER.2006.05.016.
[41] M. Rottmann, T. Beikircher, H.P Ebert, Thermal conductivity of evacuated expanded perlite measured with guarded-hot-plate and transient-hot-wire method at temperatures between 295 K and 1073 K, Int. J. Therm. Sci. 152 (2020) 106338, https://doi.org/10.1016/J.IJTHERMALSCI.2020.106338.
[42] J. Kuhn, S. Korder, M.C. Arduini-Schuster, R. Caps, J. Fricke, Infrared-optical transmission and reflection measurements on loose powders, Rev. Sci. Instrum. 64 (1998) 2523, https://doi.org/10.1063/1.1143914.
[43] R. Caps, J. Fricke, Thermal conductivity of opacified powder filler materials for vacuum insulations, Int. J. Thermophys. 21 (2000) 445–452, https://doi.org/10.1023/A:1006691731253.